ACS APPLIED MATERIALS & INTERFACES

Research Article

www.acsami.org

Evolution of the $SrTiO_3$–MoO_3 Interface Electronic Structure: An in Situ Photoelectron Spectroscopy Study

Yuanmin Du,[†] Hai Yang Peng,[‡] Hongying Mao,[§,⊥] Ke Xin Jin,[#] Hong Wang,[†] Feng Li,[†] Xing Yu Gao,[∥,▽] Wei Chen,*[,§,∥] and Tom Wu*[,†]

[†]Materials Science and Engineering, King Abdullah University of Science and Technology (KAUST), Thuwal 23955-6900, Saudi Arabia

[‡], Advanced LSI Technology Laboratory, Corporate Research and Development Center, Toshiba Corporation, Kawasaki 212-8582, Japan

[§]Department of Chemistry and [∥]Department of Physics, National University of Singapore, 2 Science Drive 3 117542, Singapore

[⊥]Department of Physics, Hangzhou Normal University, Hangzhou 310036, PR China

[#]Department of Applied Physics, Northwestern Polytechnical University, Xi'an 710072, PR China

[▽]Shanghai Institute of Applied Physics, Chinese Academy of Sciences, Shanghai 201800, PR China

ABSTRACT: Modifying the surface energetics, particularly the work function of advanced materials, is of critical importance for a wide range of surface- and interface-based devices. In this work, using in situ photoelectron spectroscopy, we investigated the evolution of electronic structure at the $SrTiO_3$ surface during the growth of ultra-thin MoO_3 layers. Because of the large work function difference between $SrTiO_3$ and MoO_3, the energy band alignment on the $SrTiO_3$ surface is significantly modified. The charge transfer and dipole formation at the $SrTiO_3$–MoO_3 interface leads to a large modulation of work function and to apparent doping in $SrTiO_3$. The measured evolutions of electronic structure and upward band bending suggest that the growth of ultra-thin MoO_3 layers is a powerful tool with which to modulate the surface energetics of $SrTiO_3$, and this surface engineering approach could be generalized to other functional oxides.

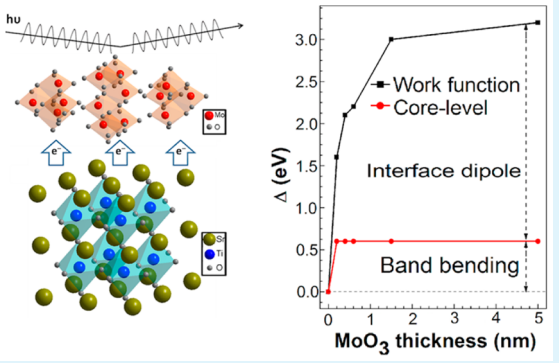

KEYWORDS: *$SrTiO_3$, MoO_3, photoelectron spectroscopy, charge transfer, work function*

INTRODUCTION

Being a prototypical perovskite-structured transition-metal oxide, $SrTiO_3$ (STO) has attracted a great deal of interest in the field of oxide electronics.[1−11] Although stoichiometric STO is an excellent band insulator with a wide band gap of 3.2−3.3 eV,[12] metallic conduction can be readily achieved by cation substitution or oxygen reduction (e.g., thermally or electrically).[13,14] Thanks to the highly tunable transport property of STO and the low activation energies of ionic migrations, a wide range of high-impact electronic devices have been realized. In particular, resistive switching devices have been demonstrated as a promising nonvolatile memory technology when the resistance states are controlled by an external electrical field.[6−10] For example, Choi et al. studied the resistive switching effect in a Pt−STO−Si heterostructure and attributed it to the change of electrical property at the Pt−STO interface as a result of interfacial charge transfer.[8] Furthermore, such interface-modulated resistive switching has been extensively reported for other transition-metal oxides.[15−22] In these breakthroughs, the electronic structures and physical properties of STO-based interfaces are important in the functionalization of oxide electronics. Hence, a deep understanding of charge transfer and interfacial band alignment is the key to further improving the performance of functional devices based on STO and other oxides. There are generally evolutions in interfacial electronic structures, particularly in charge transfer and dipole formation, when two conducting or semiconducting materials with different work functions touch.[23] Such a surface-charge-transfer doping strategy was recently applied to compound semiconductors with a focus on organic optoelectronic devices,[24] but it has not been explored for the prototypical oxide STO.

Among various metal oxides, molybdenum trioxide (MoO_3) is an environmentally friendly material that has been extensively studied in fields such as electrochromism, batteries, gas sensors, switching memories, and organic optoelectronics.[25−38] The band gap of MoO_3 has been reported to be 2.9−3.0 eV.[25,39] Oxygen deficiency in stoichiometric MoO_3 leads to occupied defect states close to the conduction band minimum, making it an n-type semiconductor. Because the Fermi level lies close to

Received: February 23, 2015
Accepted: May 12, 2015
Published: May 12, 2015

DOI: 10.1021/acsami.5b01698
ACS Appl. Mater. Interfaces 2015, 7, 11309−11314

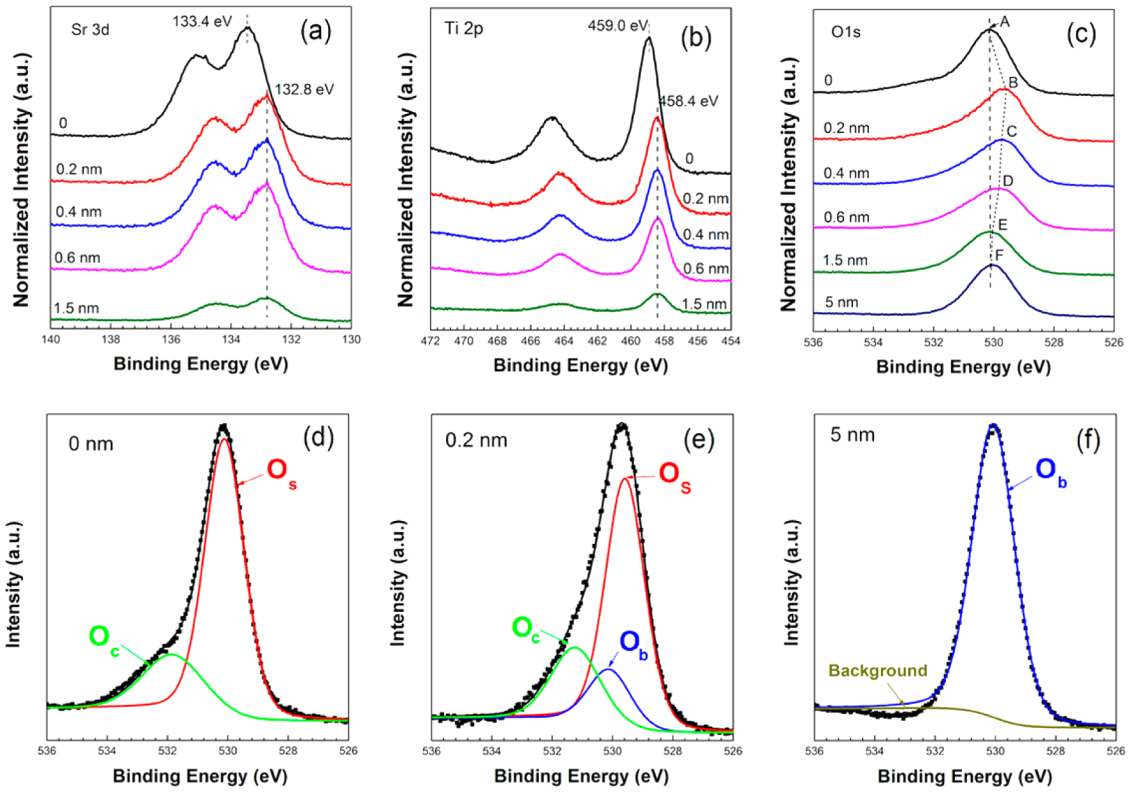

Figure 1. XPS core-level spectra during the deposition of MoO_3 on $SrTiO_3$: (a) Sr 3d, (b) Ti 2p, (c) O 1s. (d–f) O 1s spectra of a bare $SrTiO_3$ substrate and the STO–MoO_3 interfaces with nominal MoO_3 thicknesses of 0.2 and 5 nm. Solid lines represent the Gaussian–Lorentzian mixed functions used for fitting to the experimental data (black dots).

the conduction band minimum, a strong n-type semiconductor property has also been reported for MoO_3.[39] Thanks to its very high work function (6.8 eV), MoO_3 was widely used to modify the metal–organic interfaces, and a mechanism of hole injection via electron extraction has been proposed.[29−39] Furthermore, in contrast to some chemically active metals, MoO_3 is not expected to react with oxide semiconductors; thus, it is an ideal choice for investigating interfacial electronic structures.

In this report, we demonstrate effective charge transfer at the STO–MoO_3 interface as a result of the large work function difference between STO and MoO_3, and the interfacial band alignment was probed using in situ ultraviolet photoelectron spectroscopy (UPS) and X-ray photoelectron spectroscopy (XPS). To the best of our knowledge, in situ photoelectron spectroscopy techniques have not been applied to the STO–MoO_3 interface, although both materials are among the most intensively pursued oxide semiconductors. The observed evolution of charge transfer and dipole formation provides valuable insights on the properties of the STO–MoO_3 interface as a "model" system, which will facilitate the applications of STO and other oxides in advanced electronic devices.

EXPERIMENTAL SECTION

The preparation of the samples and photoelectron spectroscopy (PES) measurements were carried out in situ in a multi-chamber ultra-high-vacuum (UHV) system.[40] The 001-oriented STO single crystals (one-side polished, 10 × 10 × 0.5 mm^3) with TiO_2 termination were annealed at 650 °C in high-vacuum conditions (<10^{-7} mbar) for 10 min. The MoO_3 thin films were then thermally evaporated onto the STO substrate from a Knudsen cell in the growth chamber with a base pressure greater than 3 × 10^{-9} mbar. The deposition temperature was 400 °C and was monitored by a thermal couple at the bottom of the Knudsen cell. The deposition rate of MoO_3 (0.2 nm/min) was monitored by a quartz crystal microbalance (QCM). XPS measurements were performed with a Al Kα source ($h\nu$ = 1486.6 eV). UPS measurements were performed with He I ($h\nu$ = 21.2 eV) as the excitation source. During the UPS measurements, a sputtered clean gold foil was in contact with the sample. Binding energies of all PES spectra were referenced to the Fermi level of the gold foil. The work function of the analyzer is 4.3 eV in the UPS–XPS system. Vacuum-level shifts (changes of work function) were measured from the linear extrapolation of the low-kinetic-energy part of the UPS spectra with a −5 V sample bias.

RESULTS AND DISCUSSION

Figure 1 shows the evolution of Sr 3d, Ti 2p, and O 1s peaks as a function of increasing MoO_3 thickness on STO. The Sr 3d and the Ti 2p spectra of the clean STO surface are dominated by the Sr 3d peak centered at 133.4 ± 0.05 eV and the Ti 2p peak centered at 459.0 ± 0.05 eV, respectively. These peak positions are consistent with the report in the literature.[41] Upon the initial deposition of MoO_3 with a nominal thickness of 0.2 nm, a shift of about 0.6 eV toward lower binding energies was observed for both peaks, indicating an upward band bending or a charge (hole) transfer from MoO_3 to STO. Further increases of the MoO_3 thickness produced less notable effects on the peak shift. Because the work function of MoO_3 is much higher than that of STO, the charge transfer at the STO–MoO_3 interface is expected to result in the accumulation of holes in the STO layer. This energy shift as a result of the MoO_3 deposition is much larger than the value of 0.2 eV reported previously for the STO surface upon oxygen exposure,[42,43] indicating a much stronger electron transfer at the STO–MoO_3 interface (hole doping in STO).

DOI: 10.1021/acsami.5b01698
ACS Appl. Mater. Interfaces 2015, 7, 11309−11314

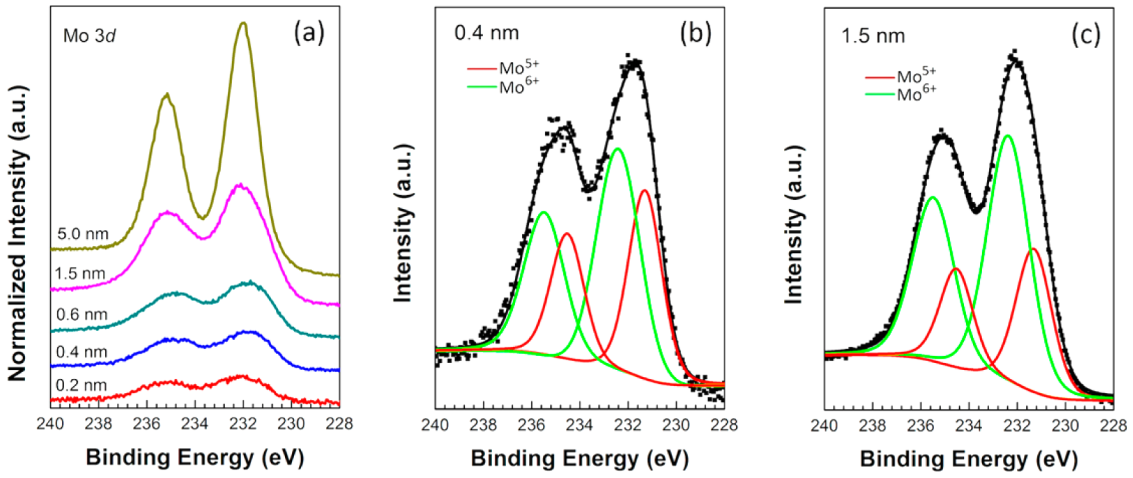

Figure 2. (a) Evolution of the Mo 3d core level as a function of the MoO_3 thickness. Fitting of the Mo 3d spectra at nominal thicknesses of (b) 0.4 and (c) 1.5 nm. The green and red lines represent Mo^{6+} and Mo^{5+} components, respectively. Solid lines and square symbols represent the fitting results and the experimental data, respectively.

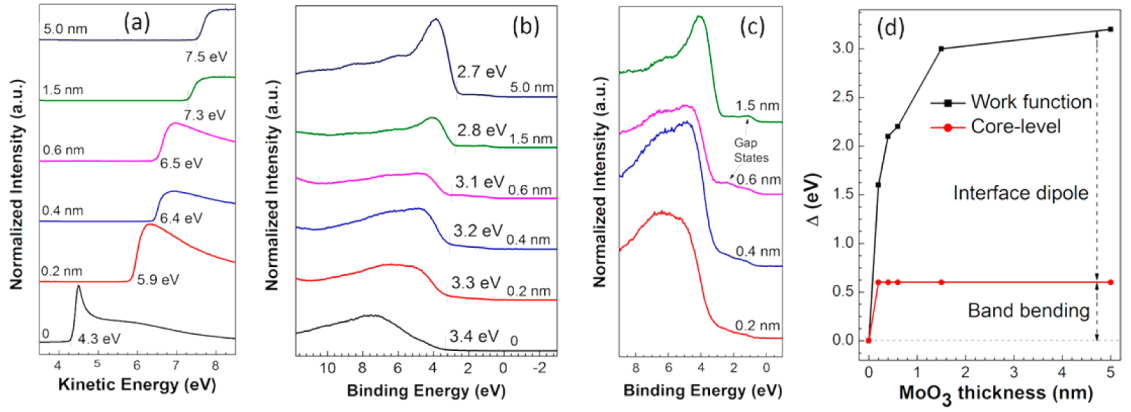

Figure 3. (a) UPS spectra in the low-kinetic-energy region (secondary electron cutoff) and (b) valence band spectra as a function of the MoO_3 thickness. (c) Close-up of the near Fermi level region of the valence band. (d) Evolutions of the work function and the core-level bending as a function of the nominal MoO_3 thickness.

The evolution of the O 1s XPS spectra gave valuable insights on the electronic structures of the STO−MoO_3 interface. Figure 1c shows the evolution of the O 1s XPS spectra as a function of MoO_3 thickness. The peak positions of the spectra are marked in Figure 1c as A−F. A notable shift to the lower binding energies was observed at the initial deposition. The peak shift was inverted at the subsequent deposition, and the O 1s peak position demonstrated an upward trend as the MoO_3 deposition thickness increased from 0.4 to 5 nm. A transition in the characteristic of the O 1s peak (symmetric → asymmetric → symmetric) was observed. To shed light on this behavior, we applied Gaussian−Lorentzian fitting to the O 1s peaks. As shown in Figure 1d, the O 1s spectrum of the bare STO substrate can be fitted with three subpeaks. The component (O_s) located at the binding energy of 530.1 eV originated from the lattice oxygen in STO, and this component shifts by 0.6 eV to a lower binding energy (529.5 eV) upon the 0.2 nm MoO_3 deposition (Figure 1e). The peak at 531.8 eV (O_c) is assigned to oxygen ions in oxygen deficient regions, i.e., oxygen vacancies.[44,45] Similar to shift in the O_s component, this peak shifts to a lower position at 531.2 eV after the MoO_3 deposition. The existence of oxygen vacancies is consistent with the high-temperature annealing process (650 °C in high-vacuum conditions for 10 min), and the oxygen vacancies donate electrons and strongly improve the STO conductivity. First-principles calculations by Shen et al.[46] showed that metallic states can be achieved by the introduction of oxygen vacancies. Using Ar^+ ion irradiation, Sánchez-Santolino et al. also reported metallic states in STO.[47] The MoO_3 deposition also leads to the appearance of a peak at 530.0 eV (O_b), as shown in Figure 1e, that is related to the lattice oxygen in MoO_3. The coexistence of O_s, O_b, and O_c leads to the asymmetric shape of the O 1s peaks. In contrast to the peak in Figure 1d, the O_s peak from the STO substrate significantly decreases after the MoO_3 deposition while the MoO_3-related O_b peak increases. When the MoO_3 thickness finally increases to 5 nm, the O 1s spectrum is dominated by the O_b component, as shown in Figure 1f. Overall, the XPS spectra indicate that multiple oxygen states are formed at the STO−MoO_3 interface, and these states evolve with the MoO_3 thickness. Furthermore, the transition between the asymmetric and symmetric characteristics of the O 1s peaks with increasing MoO_3 thickness, particularly the significant suppression of the O_c peak, indicates that substantial oxidation takes place during the MoO_3 deposition.

The transition of Mo oxidation states at the interface was further supported by the Mo 3d core-level spectra shown in Figure 2a. With the MoO_3 thicknesses of 0.4 and 1.5 nm as

DOI: 10.1021/acsami.5b01698
ACS Appl. Mater. Interfaces 2015, 7, 11309−11314

examples, the spectra are fitted with two oxidation states (i.e., Mo^{6+} and Mo^{5+} states), each composed of two peaks ($3d_{5/2}$ and $3d_{3/2}$) due to the spin−orbit splitting. In the fitted spectra shown in parts b and c of Figure 2, the energy separation between $3d_{5/2}$ and $3d_{3/2}$ was fixed at 3.1 eV. The $3d_{5/2}$ binding energies of the Mo^{6+} and Mo^{5+} states are located at 232.2 ± 0.05 and 231.3 ± 0.05 eV, respectively, which is consistent with the previous reports.[48,49] With increasing MoO_3 thickness, the regular Mo^{6+} state becomes dominant and the relative content of Mo^{5+} state decreases, indicating that the lower oxidation state mostly exists at the interface due to the electron transfer from STO to MoO_3 in the interface region. When the MoO_3 thickness increases to 5.0 nm, the Mo 3d core-level spectrum is dominated by the Mo^{6+} feature.

Understanding the interfacial energy level alignment is important for device optimization. The changes of the secondary electron cutoff with increasing MoO_3 thickness are plotted in Figure 3a. The deposition of MoO_3 on STO shifts the energy cutoff toward lower kinetic energies, i.e., increasing the "effective" work function of the STO substrate. In the measurements, an energy difference of 0.7 eV exists between the work function and the kinetic energy. Figure 3a shows that the initial STO substrate has a work function of 3.6 eV, which is close to the value reported in the literature.[50] A significant change of work function (1.6 eV) was observed at a nominal MoO_3 deposition thickness of 0.2 nm. When the MoO_3 deposition proceeds further to the thickness of 5 nm, the work function increases and finally saturates at 6.8 eV (i.e., with a large change of 3.2 eV). This final work function is the same as MoO_3,[39] indicating that bulk-like MoO_3 is formed on STO. The large work function difference between MoO_3 and STO results in a significant electron transfer from STO to MoO_3, and hence large interface dipoles form at the STO−MoO_3 interface.

Figure 3b shows the evolution of the valence band (VB) edge of STO thin films with the increasing coverage of MoO_3. The VB edge of STO is located 3.4 eV below the Fermi level. Because the SrTiO3 band gap is ~3.2 eV, the Fermi level is very close to the conduction band minimum, which is consistent with the metallic nature of the annealed STO substrate. The high-temperature annealing process produces many electron-donating oxygen vacancies, leading to the metallic state of STO. The dominant components below the edge, located between 3.0 and 10.0 eV, mainly come from the O 2p-derived states.[49,51] With increasing MoO_3 thickness, the VB edge moves closer to the Fermi level. From the VB edge of MoO_3 at 2.7 eV, an ionization energy of 9.5 eV can be derived, consistent with previous reports.[52] A close-up of the region near the Fermi level of the VB spectra (0.2 to 1.5 nm) is shown in Figure 3c. With the MoO_3 deposition, broad gap states can be clearly observed in the band gap, located between the VB edge and the Fermi level. The emergence of these gap states is consistent with the previous reports.[53−55]

In Figure 3d, the evolutions of work function and core-level banding energy are plotted as a function of the MoO_3 coverage. After a significant change at the nominal MoO_3 thickness of 0.2 nm, the work function gradually increases until a thick MoO_3 layer is formed. In contrast, after a sudden change of 0.6 eV at the initial 0.2 nm, the band bending of STO remains constant with further MoO_3 deposition. Although 0.2 nm is the minimum thickness in our experiments, we think that a gradual shift should occur for MoO_3 thicknesses smaller than 0.2 nm, and further measurements will be carried out in the future. Here, we propose that the band gap states play a key role in the evolution of the electronic structure of the STO surface. As a result of interfacial charge transfer, the oxygen vacancies on the STO side become positively charged while electrons are trapped at the gap states on the MoO_3 side, forming a negative charge zone. Such dipoles inhibit any further charge injection when the equilibrium is established, significantly affecting the electronic structure of the STO−MoO_3 interface. As shown in Figure 3d, the significant increase of the work function contains contributions from the bending of the STO band near the interface.[56] However, throughout the MoO_3 growth, the increase of the work function is substantially larger than the VB bending, indicating that the work function shift mainly comes from the interface dipoles.

The large difference in work function between STO and MoO_3 leads to significant charge transfer at the interface (Figure 4a). As a result, an electron-depleted layer is formed on

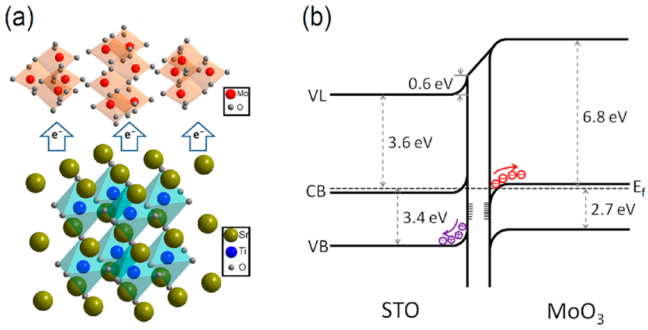

Figure 4. (a) Schematic illustration of charge transfer at the $SrTiO_3$−MoO_3 interface. (b) Energy level alignment scheme of the $SrTiO_3$−MoO_3 interface. VL, vacuum level; CB, conduction band; VB, valence band; E_f, Fermi level.

the STO side while an electron-accumulated layer is formed on the MoO_3 side. The work function of the STO substrate is significantly modulated by the ultra-thin MoO_3 layers. An energy level diagram of the STO−MoO_3 interface (based on the results of the UPS and XPS measurements) is depicted in Figure 4b. In the schematic energy diagram, band gap values of 3.2 and 2.9 eV are used for STO and MoO_3, respectively. The Fermi level is aligned across the interface in the thermodynamic equilibrium state. Initially, the STO substrate exhibits the metallic property after annealing. Upon the deposition of MoO_3, electrons transfer from STO to MoO_3; equivalently, holes are doped into the STO surface, leading to an upward band bending. As a consequence, the Fermi level at the STO surface is located between the conduction band and the valence band, indicating significant modification of the interfacial electrical property. Concurrently, the electron transfer and doping in the MoO_3 side leads to a downward band bending.

We should note that the upward band bending at the STO−MoO_3 interface observed in this work is opposite to the downward band bending extensively reported for two-dimensional electron gas formed at the STO surfaces and interfaces.[3−5] Electron-donating oxygen vacancies are extensively reported to abundantly exist in STO-related systems. However, in our experiments, the evolution of the O 1s peaks as a function of increasing MoO_3 thickness, as shown in Figure 1, indicates the occurrence of substantial oxidation and hole doping. A similar charge transfer and band-bending effect could also be induced by an electric field.[57] Thus, our report is

DOI: 10.1021/acsami.5b01698
ACS Appl. Mater. Interfaces 2015, 7, 11309−11314

complementary to these reports in the literature, and this surface transfer doping strategy clearly warrants further investigations.

As shown in Figure 4, with increasing MoO_3 thickness, large interface dipoles emerge. The underlying mechanism behind the observed maximum band bending of 0.6 eV could be due to the formation of high-density gap states at the interface, which inhibits any further hole injection into the STO surface layer. These interface states may be similar to the metal-induced gap states (MIGS) proposed for the conventional metal−semiconductor junction,[58] but more work is required to understand their physical origin and the role of interface states in the process of charge transfer. Nevertheless, the large change of work function via modulating the MoO_3 overlayer thickness provides an effective approach to control the interface barrier and the surface properties of STO-based electronic devices.

CONCLUSIONS

In summary, the electronic structure of the STO−MoO_3 interface has been investigated for the first time using in situ photoemission spectroscopy. The deposition of high-work-function MoO_3 thin film results in a hole-accumulation layer at the STO surface. A maximum band bending of 0.6 eV was observed, and the work function of STO substantially increased after the deposition of MoO_3. These results indicate the potential use of MoO_3 as an effective material to induce charge transfer and to tune the oxide work functions. This surface- and interface-engineering technique may be generalized to other oxides and heterostructures, enhancing the performance of oxide electronic devices.

AUTHOR INFORMATION

Corresponding Authors

*Email: phycw@nus.edu.sg.
*Email: tao.wu@kaust.edu.sa.

Notes

The authors declare no competing financial interest.

ACKNOWLEDGMENTS

The authors acknowledge the financial support from the Singapore MOE grant R143-000-559-112. The research reported in this publication was also supported by the King Abdullah University of Science and Technology (KAUST).

REFERENCES

(1) Mannhart, J.; Schlom, D. G. Oxide Interfaces—An Opportunity for Electronics. *Science* **2010**, *327*, 1607−1611.
(2) Son, J.; Moetakef, P.; Jalan, B.; Bierwagen, O.; Wright, N. J.; Engel-Herbert, R.; Stemmer, S. Epitaxial $SrTiO_3$ Films with Electron Mobilities Exceeding 30,000 cm^2 V^{-1} s^{-1}. *Nat. Mater.* **2010**, *9*, 482−484.
(3) Ohtomo, A.; Hwang, H. Y. A High-Mobility Electron Gas at the $LaAlO_3/SrTiO_3$ Heterointerface. *Nature* **2004**, *427*, 423−326.
(4) Santander-Syro, A. F.; Copie, O.; Kondo, T.; Fortuna, F.; Pailhès, S.; Weht, R.; Qiu, X. G.; Bertran, F.; Nicolaou, A.; Taleb-Ibrahimi, A.; Le Fèvre, P.; Herranz, G.; Bibes, M.; Reyren, N.; Apertet, Y.; Lecoeur, P.; Barthélémy, A.; Rozenberg, M. J. Two-Dimensional Electron Gas with Universal Subbands at the Surface of $SrTiO_3$. *Nature* **2011**, *469*, 189−193.
(5) Meevasana, W.; King, P. D. C.; He, R. H.; Mo, S. K.; Hashimoto, M.; Tamai, A.; Songsiriritthigul, P.; Baumberger, F.; Shen, Z.-X. Creation and Control of a Two-Dimensional Electron Liquid at the Bare $SrTiO_3$ Surface. *Nat. Mater.* **2011**, *10*, 114−118.
(6) Szot, K.; Speier, W.; Bihlmayer, G.; Waser, R. Switching the Electrical Resistance of Individual Dislocations in Single-Crystalline $SrTiO_3$. *Nat. Mater.* **2006**, *5*, 312−320.
(7) Chen, X. G.; Ma, X. B.; Yang, Y. B.; Chen, L. P.; Xiong, G. C.; Lian, G. J.; Yang, Y. C.; Yang, J. B. Comprehensive Study of the Resistance Switching in $SrTiO_3$ and Nb-Doped $SrTiO_3$. *Appl. Phys. Lett.* **2011**, *98*, 122102.
(8) Choi, D.; Lee, D.; Sim, H.; Chang, M.; Hwang, H. Reversible Resistive Switching of $SrTiO_x$ Thin Films for Nonvolatile Memory Applications. *Appl. Phys. Lett.* **2006**, *88*, 082904.
(9) Wu, S.; Luo, X.; Turner, S.; Peng, H.; Lin, W.; Ding, J.; David, A.; Wang, B.; Van Tendeloo, G.; Wang, J.; Wu, T. Nonvolatile Resistive Switching in $Pt/LaAlO_3/SrTiO_3$ Heterostructures. *Phys. Rev. X* **2013**, *3*, 041027.
(10) Peng, H. Y.; Pu, L.; Wu, J. C.; Cha, D.; Hong, J. H.; Lin, W. N.; Li, Y. Y.; Ding, J. F.; David, A.; Li, K.; Wu, T. Effects of Electrode Material and Configuration on the Characteristics of Planar Resistive Switching Devices. *APL Mater.* **2013**, *1*, 052106.
(11) Chen, Y. Z.; Bovet, N.; Trier, F.; Christensen, D. V.; Qu, F. M.; Andersen, N. H.; Kasama, T.; Zhang, W.; Giraud, R.; Dufouleur, J.; Jespersen, T. S.; Sun, J. R.; Smith, A.; Nygård, J.; Lu, K.; Büchner, B.; Shen, B. G.; Linderoth, S.; Pryds, N. A High-Mobility Two-Dimensional Electron Gas at the Spinel/Perovskite Interface of γ-$Al_2O_3/SrTiO_3$. *Nat. Commun.* **2013**, *4*, 1371.
(12) Van Benthem, K.; Elsäesser, C.; French, R. H. Bulk Electronic Structure of SrTiO3: Experiment and Theory. *J. Appl. Phys.* **2001**, *90*, 6156−6164.
(13) Jin, K. X.; Li, Y. F.; Wang, Z. L.; Peng, H. Y.; Lin, W. N.; Kyaw, A. K. K.; Jin, Y. L.; Jin, K. J.; Sun, X. W.; Soci, C.; Wu, T. Tunable Photovoltaic Effect and Solar Cell Performance of Self-Doped Perovskite $SrTiO_3$. *AIP Adv.* **2012**, *2*, 042131.
(14) Bera, A.; Peng, H.; Lourembam, J.; Shen, Y.; Sun, X. W.; Wu, T. A Versatile Light-Switchable Nanorod Memory: Wurtzite ZnO on Perovskite $SrTiO_3$. *Adv. Funct. Mater.* **2013**, *23*, 4977−4984.
(15) Sawa, A. Resistive Switching in Transition Metal Oxides. *Mater. Today* **2008**, *11*, 28−36.
(16) Du, Y. M.; Pan, H.; Wang, S. J.; Wu, T.; Feng, Y. P.; Pan, J. S.; Wee, A. T. S. Symmetrical Negative Differential Resistance Behavior of a Resistive Switching Device. *ACS Nano* **2012**, *6*, 2517−2523.
(17) Zazpe, R.; Stoliar, P.; Golmar, F.; Llopis, R.; Casanova, F.; Hueso, L. E. Resistive Switching in Rectifying Interfaces of Metal−Semiconductor−Metal Structures. *Appl. Phys. Lett.* **2013**, *103*, 073114.
(18) Wu, S.; Ren, L.; Qing, J.; Yu, F.; Yang, K.; Yang, M.; Wang, Y.; Meng, M.; Zhou, W.; Zhou, X.; Li, S. Bipolar Resistance Switching in Transparent $ITO/LaAlO_3/SrTiO_3$ Memristors. *ACS Appl. Mater. Interfaces* **2014**, *6*, 8575−8579.
(19) Lee, H.; Kim, H.; Van, T. N.; Kim, D.-W.; Park, J. Y. Nanoscale Resistive Switching Schottky Contacts on Self-Assembled Pt Nanodots on $SrTiO_3$. *ACS Appl. Mater. Interfaces* **2013**, *5*, 11668−11672.
(20) Du, Y. M.; Kumar, A.; Pan, H.; Zeng, K. Y.; Wang, S. J.; Yang, P.; Wee, A. T. S. The Resistive Switching in TiO_2 Films Studied by Conductive Atomic Force Microscopy and Kelvin Probe Force Microscopy. *AIP Adv.* **2013**, *3*, 082107.
(21) Cui, Y.; Peng, H. Y.; Wu, S.; Wang, R.; Wu, T. Complementary Charge Trapping and Ionic Migration in Resistive Switching of Rare-Earth Manganite $TbMnO_3$. *ACS Appl. Mater. Interfaces* **2013**, *5*, 1213−1217.
(22) Peng, H. Y.; Li, Y. F.; Lin, W. N.; Wang, Y. Z.; Gao, X. Y.; Wu, T. Deterministic Conversion between Memory and Threshold Resistive Switching via Tuning the Strong Electron Correlation. *Sci. Rep.* **2012**, *2*, 442.
(23) Sze, S. M. *Semiconductor Devices, Physics, and Technology*, 2nd ed; Wiley & Sons, Inc.: New York, 2002.
(24) Chen, W.; Qi, D. C.; Gao, X. Y.; Wee, A. T. S. Surface Transfer Doping of Semiconductors. *Prog. Surf. Sci.* **2009**, *84*, 279−321.
(25) Patil, P. S.; Patil, R. S. Studies on Spray Pyrolyzed Molybdenum Trioxide Thin Films. *Bull. Mater. Sci.* **1995**, *18*, 911−916.

DOI: 10.1021/acsami.5b01698
ACS Appl. Mater. Interfaces 2015, 7, 11309−11314

(26) Hassan, M. F.; Guo, Z. P.; Chen, Z.; Liu, H. K. Carbon-Coated MoO_3 Nanobelts as Anode Materials for Lithium-Ion Batteries. *J. Power Sources* **2010**, *195*, 2372−2376.
(27) Yu, J.; Ippolito, S. J.; Shafiei, M.; Dhawan, D.; Wlodarski, W.; Kalantar-zadeh, K. Reverse Biased Pt/Nanostructured MoO_3/SiC Schottky Diode Based Hydrogen Gas Sensors. *Appl. Phys. Lett.* **2009**, *94*, 013504.
(28) Bessonov, A. A.; Kirikova, M. N.; Petukhov, D. I.; Allen, M.; Ryhänen, T.; Bailey, M. J. A. Layered Memristive and Memcapacitive Switches for Printable Electronics. *Nat. Mater.* **2015**, *14*, 199−204.
(29) Liang, J.; Zu, F. S.; Ding, L.; Xu, M. F.; Shi, X. B.; Wang, Z. K.; Liao, L. S. Aqueous Solution-Processed MoO_3 Thick Films as Hole Injection and Short-Circuit Barrier Layer in Large-Area Organic Light-Emitting Devices. *Appl. Phys. Express* **2014**, *7*, 111601.
(30) Liu, L. Y.; Wan, L.; Cao, L.; Han, Y. Y.; Zhang, W. H.; Chen, T. X.; Guo, P. P.; Wang, K.; Xu, F. Q. Assistance of Partially Reduced MoO_3 Interlayer to Hole-Injection at Iron Phthalocyanine/ITO Interface Evidenced by Photoemission Study. *Appl. Surf. Sci.* **2013**, *271*, 352−356.
(31) Fu, Q.; Chen, J. S.; Shi, C. S.; Ma, D. G. Room-Temperature Sol-Gel Derived Molybdenum Oxide Thin Films for Efficient and Stable Solution-Processed Organic Light-Emitting Diodes. *ACS Appl. Mater. Interfaces* **2013**, *5*, 6024−6029.
(32) Douvas, A. M.; Vasilopoulou, M.; Georgiadou, D. G.; Soultati, A.; Davazoglou, D.; Vourdas, N.; Giannakopoulos, K. P.; Kontos, A. G.; Kennou, S.; Argitis, P. Sol−gel Synthesized, Low-Temperature Processed, Reduced Molybdenum Peroxides for Organic Optoelectronics Applications. *J. Mater. Chem. C* **2014**, *2*, 6290−6300.
(33) Wong, K. H.; Ananthanarayanan, K.; Luther, J.; Balaya, P. Origin of Hole Selectivity and the Role of Defects in Low-Temperature Solution-Processed Molybdenum Oxide Interfacial Layer for Organic Solar Cells. *J. Phys. Chem. C* **2012**, *116*, 16346−16351.
(34) Hancox, I.; Rochford, L. A.; Clare, D.; Walker, M.; Mudd, J. J.; Sullivan, P.; Schumann, S.; McConville, C. F.; Jones, T. S. Optimization of a High Work Function Solution Processed Vanadium Oxide Hole-Extracting Layer for Small Molecule and Polymer Organic Photovoltaic Cells. *J. Phys. Chem. C* **2013**, *117*, 49−57.
(35) Dong, W. J.; Jung, G. H.; Lee, J. L. Solution-Processed-MoO_3 Hole Extraction Layer on Oxygen Plasma-Treated Indium Tin Oxide in Organic Photovoltaics. *Sol. Energy Mater. Sol. Cells* **2013**, *116*, 94−101.
(36) Tao, C.; Ruan, S. P.; Zhang, X. D.; Xie, G. H.; Shen, L.; Kong, X. Z.; Dong, W.; Liu, C. X.; Chen, W. Y. Performance Improvement of Inverted Polymer Solar Cells with Different Top Electrodes by Introducing a MoO_3 Buffer Layer. *Appl. Phys. Lett.* **2008**, *93*, 193307.
(37) Lu, M.; Shao, C.; Wang, K.; Lu, N.; Zhang, X.; Zhang, P.; Zhang, M.; Li, X.; Liu, Y. *p*-MoO_3 Nanostructures/*n*-TiO_2 Nanofiber Heterojunctions: Controlled Fabrication and Enhanced Photocatalytic Properties. *ACS Appl. Mater. Interfaces* **2014**, *6*, 9004−9012.
(38) Zhou, Y. L.; Holmes, R. J. Influence of a MoO_x Interlayer on the Open-Circuit Voltage in Organic Photovoltaic Cells. *Appl. Phys. Lett.* **2013**, *103*, 053302.
(39) Kröger, M.; Hamwi, S.; Meyer, J.; Riedl, T.; Kowalsky, W.; Kahn, A. Role of the Deep-Lying Electronic States of MoO_3 in the Enhancement of Hole Injection in Organic Thin Films. *Appl. Phys. Lett.* **2009**, *95*, 123301.
(40) Zhong, J. Q.; Huang, H.; Mao, H. Y.; Wang, R.; Zhong, S.; Chen, W. Molecular-Scale Investigation of C_{60}/*p*-Sexiphenyl Organic Heterojunction Interface. *J. Chem. Phys.* **2011**, *134*, 154706.
(41) Van der Heide, P. A. W.; Jiang, Q. D.; Kim, Y. S.; Rabalais, J. W. X-ray Photoelectron Spectroscopic and Ion Scattering Study of the $SrTiO_3$ (0 0 1) Surface. *Surf. Sci.* **2001**, *473*, 59−70.
(42) Aiura, Y.; Hase, I.; Bando, H.; Yasue, T.; Saitoh, T.; Dessau, D. S. Photoemission Study of the Metallic State of Lightly Electron-Doped $SrTiO_3$. *Surf. Sci.* **2002**, *515*, 61−74.
(43) Henrich, V. E.; Dresselhaus, G.; Zeiger, H. J. Chemisorbed Phases of O_2 on TiO_2 and $SrTiO_3$. *J. Vac. Sci. Technol. (New York, NY)* **1978**, *15*, 534−537.
(44) Chen, M.; Wang, X.; Yu, Y. H.; Pei, Z. L.; Bai, X. D.; Sun, C.; Huang, R. F.; Wen, L. S. X-ray Photoelectron Spectroscopy and Auger Electron Spectroscopy Studies of Al-Doped ZnO Films. *Appl. Surf. Sci.* **2000**, *158*, 134−140.
(45) Yang, G. J.; Gao, D. Q.; Shi, Z. H.; Zhang, Z. H.; Zhang, J.; Zhang, J. L.; Xue, D. S. Room Temperature Ferromagnetism in Vacuum-Annealed CoO Nanospheres. *J. Phys. Chem. C* **2000**, *114*, 21989−21993.
(46) Shen, J.; Lee, H.; Valentí, R.; Jeschke, H. O. Ab Initio Study of the Two-Dimensional Metallic State at The Surface of $SrTiO_3$: Importance of Oxygen Vacancies. *Phys. Rev. B: Condens. Matter Mater. Phys.* **2012**, *86*, 195119.
(47) Sánchez-Santolino, G.; Tornos, J.; Bruno, F. Y.; Cuellar, F. A.; Leon, C.; Santamaría, J.; Pennycook, S. J.; Varela, M. Characterization of Surface Metallic States in $SrTiO_3$ by Means of Aberration Corrected Electron Microscopy. *Ultramicroscopy* **2013**, *127*, 109−113.
(48) Bhosle, V.; Tiwari, A.; Narayan, J. Epitaxial Growth and Properties of MoO_x ($2 < x < 2.75$) Films. *J. Appl. Phys.* **2005**, *97*, 083539.
(49) Fleisch, T. H.; Mains, G. J. An XPS Study of the UV Reduction and Photochromism of MoO_3 and WO_3. *J. Chem. Phys.* **1982**, *76*, 780−786.
(50) Robertson, J.; Chen, C. W. Schottky Barrier Heights of Tantalum Oxide, Barium Strontium Titanate, Lead Ttitanate, and Strontium Bismuth Tantalite. *Appl. Phys. Lett.* **1999**, *74*, 1168−1170.
(51) Wu, C. I.; Lin, C. T.; Lee, G. R.; Cho, T. Y.; Wu, C. C. Pi, T. W. Electronic and Chemical Properties of Molybdenum Oxide Doped Hole Injection Layers in Organic Light Emitting Diodes. *J. Appl. Phys.* **2009**, *105*, 033717.
(52) Kröger, M.; Hamwi, S.; Meyer, J.; Riedl, T.; Kowalsky, W.; Kahn, A. P-Type Doping of Organic Wide Band Gap Materials by Transition Metal Oxides: A Case-Study on Molybdenum Trioxide. *Org. Electron.* **2009**, *10*, 932−938.
(53) Kanai, K.; Koizumi, K.; Ouchi, S.; Tsukamoto, Y.; Sakanoue, K.; Ouchi, Y.; Seki, K. Electronic Structure of Anode Interface with Molybdenum Oxide Buffer Layer. *Org. Electron.* **2010**, *11*, 188−194.
(54) Tokarz-Sobieraj, R.; Hermann, K.; Witko, M.; Blume, A.; Mestl, G.; Schlogl, R. Properties of Oxygen Sites at the MoO_3 (0 1 0) Surface: Density Functional Theory Cluster Studies and Photoemission Experiments. *Surf. Sci.* **2001**, *489*, 107−125.
(55) Lee, H.; Cho, S. W.; Han, K.; Jeon, P. E.; Whang, C.-N.; Jeong, K.; Cho, K.; Yi, Y. The Origin of the Hole Injection Improvements at Indium Tin Oxide/Molybdenum Trioxide/*N*,*N*′-bis(1-Naphthyl)-*N*,*N*′-diphenyl-1,1′-biphenyl-4,4′-diamine Interfaces. *Appl. Phys. Lett.* **2008**, *93*, 043308.
(56) Cahen, D.; Kahn, A. Electron Energetics at Surfaces and Interfaces: Concepts and Experiments. *Adv. Mater.* **2003**, *15*, 271−277.
(57) Lin, W.; Ding, J.; Wu, S.; Li, Y.; Lourembam, J.; Shannigrahi, S.; Wang, S.; Wu, T. Electrostatic modulation of $LaAlO_3$/$SrTiO_3$ Interface Transport in an Electric Double-Layer Transistor. *Adv. Mater. Interfaces* **2014**, *1*, 1300001.
(58) Tersoff, J. Schottky Barrier Heights and the Continuum of Gap States. *Phys. Rev. Lett.* **1984**, *52*, 465−468.

DOI: 10.1021/acsami.5b01698
ACS Appl. Mater. Interfaces 2015, 7, 11309−11314